AMES GRANT
IN-02-CR
106602

FINAL REPORT

P.29

NASA Grant NAG 2–502

February 1, 1988 – January 31, 1992

DEVELOPMENT OF A 3-D UPWIND PNS CODE FOR CHEMICALLY REACTING HYPERSONIC FLOWFIELDS

by

J. C. Tannehill, Principal Investigator
G. Wadawadigi
Iowa State University
Ames, Iowa 50010

Submitted to: National Aeronautics and Space Administration
Ames Research Center
Moffett Field, California

(NASA-CR-190182) DEVELOPMENT OF A 3-D UPWIND PNS CODE FOR CHEMICALLY REACTING HYPERSONIC FLOWFIELDS Final Report, 1 Feb. 1988 - 31 Jan. 1992 (Iowa State Univ. of Science and Technology) 29 p

N92-30977

Unclas

G3/02 0106602

ERI Project 3051
CFD 26

FINAL REPORT

NASA Grant NAG 2–502

February 1, 1988 – January 31, 1992

DEVELOPMENT OF A 3-D UPWIND PNS CODE FOR CHEMICALLY REACTING HYPERSONIC FLOWFIELDS

by

J. C. Tannehill, Principal Investigator
G. Wadawadigi
Iowa State University
Ames, Iowa 50010

Submitted to: National Aeronautics and Space Administration
Ames Research Center
Moffett Field, California

ERI Project 3051
CFD 26

SUMMARY

This final report summarizes the research accomplished under NASA Grant NAG 2–502 during the entire funded period which extended from February 1, 1988 to January 31, 1992. The total funding amounted to $173,625. The Technical Officers for this grant were Michael J. Green and Thomas A. Edwards of NASA Ames Research Center.

INTRODUCTION

The research performed during this grant represents a continuation of the work initiated under the NASA Grants NAG 2–245 and NAS2–12861. During these grants, two new parabolized Navier–Stokes (PNS) codes have been developed to compute the three–dimensional, viscous, chemically reacting flow of air around hypersonic vehicles such as the National Aero-Space Plane (NASP).

The first code (TONIC), originally developed by Prabhu et al. [1,2], solves the gas dynamic and species conservation equations in a fully coupled manner using an implicit, approximately–factored, central–difference algorithm. During the present grant, this code was upgraded [3] to include shock fitting and the capability of computing the flow around complex body shapes. The revised TONIC code was validated by computing the chemically–reacting (M_∞=25.3) flow around a 10° half–angle cone at various angles of attack and the Ames All–Body model at 0° angle of attack. The results of these calculations [3] were in good agreement with the results from the UPS code. One of the major drawbacks of the TONIC code is that the central–differencing of fluxes across interior flowfield discontinuities tends to introduce errors into the solution in the form of local flow property oscillations. In order to control these oscillations, some type of artificial dissipation is required. The correct magnitude of this added smoothing is generally left for the user to specify through a trial-and-error process.

The second code (UPS), originally developed by Lawrence et al. [4,5] for a perfect gas, has been extended by Tannehill et al. [6–9] to permit either perfect gas, equilibrium air, or

nonequilibrium air computations. The code solves the PNS equations using a finite–volume, upwind TVD method based on Roe's approximate Riemann solver that has been modified to account for real gas effects using the approach of Grossman and Walters [10]. The dissipation term associated with this algorithm is sufficiently adaptive to flow conditions that, even when attempting to capture very strong shock waves, no additional smoothing is required. For nonequilibrium calculations, the code solves the fluid dynamic and species continuity equations in a loosely–coupled manner. The fluid medium is assumed to be a chemically reacting mixture of thermally perfect (but calorically imperfect) gases in thermal equilibrium. This code was used to calculate the hypersonic, laminar flow of chemically reacting air over cones at various angles of attack. In addition, the flow around the McDonnell Douglas generic option blended-wing-body was computed [9] and comparisons were made between the perfect gas, equilibrium air, and the nonequilibrium air results.

The TONIC and UPS codes have been carefully compared during the present grant. During these comparison tests, [3,11] it became evident that the UPS code is much more robust than the TONIC code and requires less user interaction. In addition, it was noted that the loosely–coupled approach used in the UPS code permits different chemistry models to be readily inserted. As a result of the comparison tests, it was decided to discontinue the development of the TONIC code while continuing the development of the UPS code.

The UPS code has since been extended in the present grant to permit internal turbulent flow calculations with hydrogen–air chemistry. The chemistry model contains eleven reactions and nine species and is based on the NASP model [12]. With these additions, the new code has the capability of computing both aerodynamic and propulsive flowfields. This capability is required in order to successfully analyze the scramjet propulsion system employed on the National Aero-Space Plane. The new code has been applied to two internal flow test cases. The first case consists of the Burrows–Kurkov supersonic combustion experiment [13] in which hydrogen was injected tangentially at sonic speed through a slot in the floor of a test section with a M_∞=2.44 vitiated airstream. In the second test case, the code was used

to compute a generic 3–D scramjet (M_∞=7.0) flowfield.

GOVERNING EQUATIONS

The PNS equations are used in the present research to model the fluid dynamics. These are obtained from the steady, compressible Navier–Stokes equations by neglecting streamwise viscous terms and by retaining only a fraction of the streamwise pressure gradient term in the subsonic layer in order to eliminate ellipticity in the marching direction. The latter is accomplished using Vigneron's technique [14] in conjunction with the extension to chemically–reacting flows by Prabhu *et al.* [2]. The PNS equations expressed in generalized coordinates (ξ, η, ζ) are given by

$$\mathbf{E}_\xi + \mathbf{F}_\eta + \mathbf{G}_\zeta = 0 \tag{1}$$

where

$$\begin{aligned}
\mathbf{E} &= \left(\frac{\xi_x}{J}\right)\mathbf{E}_i + \left(\frac{\xi_y}{J}\right)\mathbf{F}_i + \left(\frac{\xi_z}{J}\right)\mathbf{G}_i \\
\mathbf{F} &= \left(\frac{\eta_x}{J}\right)(\mathbf{E}_i - \mathbf{E}_v^*) + \left(\frac{\eta_y}{J}\right)(\mathbf{F}_i - \mathbf{F}_v^*) + \left(\frac{\eta_z}{J}\right)(\mathbf{G}_i - \mathbf{G}_v^*) \\
\mathbf{G} &= \left(\frac{\zeta_x}{J}\right)(\mathbf{E}_i - \mathbf{E}_v^*) + \left(\frac{\zeta_y}{J}\right)(\mathbf{F}_i - \mathbf{F}_v^*) + \left(\frac{\zeta_z}{J}\right)(\mathbf{G}_i - \mathbf{G}_v^*)
\end{aligned} \tag{2}$$

The inviscid and viscous flux vectors are given by

$$\begin{aligned}
\mathbf{E}_i &= \left\{\rho u, \rho u^2 + p, \rho uv, \rho uw, (E_t + p)\,u\right\}^T \\
\mathbf{F}_i &= \left\{\rho v, \rho uv, \rho v^2 + p, \rho vw, (E_t + p)\,v\right\}^T \\
\mathbf{G}_i &= \left\{\rho w, \rho uw, \rho vw, \rho w^2 + p, (E_t + p)\,w\right\}^T \\
\mathbf{E}_v &= \{0, \tau_{xx}, \tau_{xy}, \tau_{xz}, u\tau_{xx} + v\tau_{xy} + w\tau_{xz} - q_x\}^T \\
\mathbf{F}_v &= \{0, \tau_{yx}, \tau_{yy}, \tau_{yz}, u\tau_{yx} + v\tau_{yy} + w\tau_{yz} - q_y\}^T \\
\mathbf{G}_v &= \{0, \tau_{zx}, \tau_{zy}, \tau_{zz}, u\tau_{zx} + v\tau_{zy} + w\tau_{zz} - q_z\}^T
\end{aligned} \tag{3}$$

where $E_t = \rho\{e + \frac{1}{2}(u^2 + v^2 + w^2)\}$

where the non-dimensional quantity β_3 is

$$\beta_3 = \frac{\rho^*_\infty \mathcal{D}^*_\infty}{\mu^*_\infty \mathrm{Re}_\infty}$$

and $\mathcal{D}_{sm}$ is the multicomponent diffusion coefficient for the species s. In the present work a kinetic binary diffusion coefficient $\mathcal{D}$ is used and is assumed to be the same for all the species. The species continuity equation is simplified using the PNS approximation of dropping the unsteady term and neglecting the streamwise diffusion terms. After recasting the equation into generalized coordinates, the final form is obtained:

$$\rho\hat{U}\frac{\partial c_s}{\partial \xi} + \rho\hat{V}\frac{\partial c_s}{\partial \eta} + \rho\hat{W}\frac{\partial c_s}{\partial \zeta} - \frac{\partial}{\partial \eta}\left[A_{\eta\eta}\frac{\partial c_s}{\partial \eta} + A_{\eta\zeta}\frac{\partial c_s}{\partial \zeta}\right]$$
$$- \frac{\partial}{\partial \zeta}\left[A_{\zeta\zeta}\frac{\partial c_s}{\partial \zeta} + A_{\zeta\eta}\frac{\partial c_s}{\partial \eta}\right] = \frac{\dot{\omega}_s}{J} \tag{7}$$

where

$$\begin{aligned}
\hat{U} &= \left(\frac{\xi_x}{J}\right)u + \left(\frac{\xi_y}{J}\right)v + \left(\frac{\xi_z}{J}\right)w \\
\hat{V} &= \left(\frac{\eta_x}{J}\right)u + \left(\frac{\eta_y}{J}\right)v + \left(\frac{\eta_z}{J}\right)w \\
\hat{W} &= \left(\frac{\zeta_x}{J}\right)u + \left(\frac{\zeta_y}{J}\right)v + \left(\frac{\zeta_z}{J}\right)w
\end{aligned} \tag{8}$$

and

$$\begin{aligned}
A_{\eta\eta} &= \beta_3\rho\mathcal{D}\left[\frac{\eta_x^2}{J} + \frac{\eta_y^2}{J} + \frac{\eta_z^2}{J}\right] \\
A_{\zeta\zeta} &= \beta_3\rho\mathcal{D}\left[\frac{\zeta_x^2}{J} + \frac{\zeta_y^2}{J} + \frac{\zeta_z^2}{J}\right] \\
A_{\eta\zeta} = A_{\zeta\eta} &= \beta_3\rho\mathcal{D}\left[\frac{\eta_x\zeta_x}{J} + \frac{\eta_y\zeta_y}{J} + \frac{\eta_z\zeta_z}{J}\right]
\end{aligned} \tag{9}$$

In addition to the above equations, the equation of state is used:

$$p = \frac{\beta_1\rho T}{\mathcal{M}} \tag{10}$$

where the nondimensional quantity β_1 and molecular weight of the mixture $\mathcal{M}$ are given by

$$\beta_1 = \frac{\mathcal{R}_U^* T_\infty^*}{\mathcal{M}_\infty^* V_\infty^{*2}}, \qquad \mathcal{M} = \left(\sum_{s=1}^{n} \frac{c_s}{\mathcal{M}_s} \right)^{-1}$$

and $\mathcal{R}_U$ is the unversal gas constant (8314.34 J/kmol/K). The ratio of specific heats, γ is defined as

$$\gamma = 1 + \left(\frac{p}{\rho e^s} \right) \tag{11}$$

where e^s is the sensible energy which can be expressed in terms of the species mass fractions (c_s) and the species formation enthalpy at 0°K ($h_{f_s}^0$) by

$$e^s = e - \sum_{s=1}^{n} c_s h_{f_s}^0$$

In addition, the following nondimensional quantities are used

$$\mathcal{M} = \frac{\mathcal{M}^*}{\mathcal{M}_\infty} \qquad C_{p_f} = \frac{C_{p_f}^* T_\infty^*}{V_\infty^{*2}}$$

$$\dot{\omega}_s^* = \frac{\dot{\omega}_s^*}{\rho_\infty^* V_\infty^*} \qquad \mathcal{D} = \frac{\mathcal{D}^*}{\mathcal{D}_\infty^*}$$

Thermodynamic and Transport Properties

Enthalpy and specific heat

The enthalpy and specific heat are obtained from a table lookup procedure using the data of Ref. [15]. Cubic spline interpolation is used to the find the property at a particular temperature. Since the enthalpies in Ref. [15] are referenced to 298.15°K, they are re-referenced to 0°K in the following manner. For each species, the enthalpy at 0°K is subtracted from the enthalpy at a particular temperature T (all referenced to 298.15°K). This yields the sensible enthalpy referenced to 0°K at the temperature T. The species formation enthalpy at 0°K is then added to obtain the properly referenced enthalpy. The enthalpy and frozen specific heat of the mixture are given by

$$h^* = \sum_{s=1}^{n} c_s h_s^* \tag{12}$$

$$C_{p_f}^* = \left. \frac{dh^*}{dT^*} \right|_{c_1,\ldots,c_n} = \sum_{s=1}^{n} c_s \frac{dh_s^*}{dT^*} = \sum_{s=1}^{n} c_s C_{p,s}^*$$

where the subscripts on the differentiation denote that the mixture composition is locally frozen.

Viscosity and Thermal Conductivity

Cubic spline interpolation is employed to obtain the species viscosity, μ_s, from the tabulated data given in Ref. [16]. The thermal conductivity of species s is computed using Eucken's semiempirical formula

$$\kappa_s^* = \frac{\mu_s^* \mathcal{R}^*}{\mathcal{M}_s^*} \left(C_{p,s}^* \frac{\mathcal{M}_s^*}{\mathcal{R}^*} + \frac{5}{4} \right)$$

The viscosity and thermal conductivity of the mixture are calculated using Wilke's semiempirical mixing rule [17].

$$\mu^* = \sum_{s=1}^{n} \frac{\mathrm{X}_s \mu_s^*}{\phi_s} \quad , \quad \kappa^* = \sum_{s=1}^{n} \frac{\mathrm{X}_s \kappa_s^*}{\phi_s} \tag{13}$$

where

$$\mathrm{X}_s = \frac{c_s \mathcal{M}^*}{\mathcal{M}_s^*}$$

$$\phi_s = \sum_{r=1}^{n} \mathrm{X}_r \left[1 + \sqrt{\frac{\mu_s^*}{\mu_r^*}} \left(\frac{\mathcal{M}_r^*}{\mathcal{M}_s^*} \right)^{\frac{1}{4}} \right]^2 \left[\sqrt{8} \sqrt{1 + \frac{\mathcal{M}_r^*}{\mathcal{M}_s^*}} \right]^{-1}$$

Diffusion coefficient

The binary Lewis number, $\mathcal{L}e$, is assumed to be the same constant for all the species and is taken to be unity [18] for the present calculations. The kinematic diffusion coefficient $\mathcal{D}^*$ is then computed from the definition

$$\mathcal{D}^* = \frac{\kappa^* \mathcal{L}e}{\rho^* C_{p_f}^*} \tag{14}$$

Chemistry Model

A eleven reaction/nine species hydrogen–air chemistry model is employed. The reactions and the corresponding forward reaction rate variables are based on the NASP model [12] and are given in Table 1. The forward reaction rate for the kth reaction is expressed in the following expanded Arrhenius form:

$$K_{f,k}^*(T^*) = A T^{*^n} \exp(-\Theta / T^*) \tag{15}$$

	Reaction	A	n	Θ
1	$H + O_2 \rightleftharpoons O + OH$	1.91E+14	0	8273
2	$O + H_2 \rightleftharpoons H + OH$	5.06E+04	2.67	3166
3	$OH + OH \rightleftharpoons O + H_2O$	1.50E+09	1.14	0
4	$OH + H_2 \rightleftharpoons H + H_2O$	2.16E+08	1.51	1726
5	$O + NO \rightleftharpoons N + O_2$	3.80E+09	1.0	20820
6	$O + N_2 \rightleftharpoons NO + N$	1.82E+14	0	38370
7	$H + NO \rightleftharpoons N + OH$	1.70E+14	0	24560
8	$H + H + M \rightleftharpoons H_2 + M$	7.30E+17	-1.0	0
9	$H + O + M \rightleftharpoons OH + M$	2.60E+16	-0.6	0
10	$O + O + M \rightleftharpoons O_2 + M$	1.14E+17	-1.0	0
11	$H + OH + M \rightleftharpoons H_2O + M$	8.62E+21	-2.0	0

Table 1: Reactions and reaction rates

In Table 1 the units for the forward reaction rates are cm^3/mol-sec or cm^6/mol^2-sec and the third-body efficiencies are 2.5 for M=H_2, 16.25 for M=H_2O and 1.0 for all other M.

The above model of eleven reactions ($m = 11$), nine species ($n = 9$) and ten reactants ($n_t = 10$) can be symbolically represented as:

$$\sum_{l=1}^{n_t} \nu'_{k,l} A_l \rightleftharpoons \sum_{l=1}^{n_t} \nu''_{k,l} A_l, \qquad k = 1, 2, \ldots, m \tag{16}$$

where $\nu'_{k,l}$ and $\nu''_{k,l}$ are the stoichiometric coefficients and A_l is the chemical symbol of the lth species. Using the law of mass action, the mass production/depletion rate of the species s is

$$\dot{\omega}^*_s = \mathcal{M}^*_s \sum_{k=1}^{m} \left(\nu''_{k,s} - \nu'_{k,l}\right) \left\{ K^*_{f,k}(T^*) \prod_{r=1}^{n_t} [\rho^* \gamma^*_r]^{\nu'_{k,r}} - K^*_{b,k}(T^*) \prod_{r=1}^{n_t} [\rho^* \gamma^*_r]^{\nu''_{k,r}} \right\} \tag{17}$$

The mole–mass ratios of the reactants are defined as

$$\gamma^*_r = \begin{cases} c_r / \mathcal{M}^*_r, & r = 1, 2, \ldots, n \\ \sum_{s=1}^{n} Z_{r,s} \gamma^*_s, & r = n+1, \ldots, n_t \end{cases} \tag{18}$$

where $Z_{r,s}$ are the third-body efficiencies for each of the species. The backward reaction rate required for $\dot{\omega}_s^*$ is obtained from

$$K_{b,k}^* = \frac{K_{f,k}^*}{K_{eq,k}^*}, \quad k = 1, 2, \ldots, m \tag{19}$$

where $K_{eq,k}^*$ is the equilibrium constant of the kth reaction given by

$$K_{eq,k}^* = \left(\mathcal{R}_U' T^*\right)^{-\Delta n_k} \exp\left(\frac{-\Delta G_k^*}{\mathcal{R}_U T^*}\right) \tag{20}$$

where $\mathcal{R}_U' = 82.06 \times 10^{-6}\text{m}^3\text{atm/mol-°K}$ [19] and Δn_k is the integer difference between the numbers of product and reactant species:

$$\Delta n_k = \sum_{s=1}^{n} \nu_{k,s}'' - \sum_{s=1}^{n} \nu_{k,s}' \tag{21}$$

and

$$\Delta G_k^* = \sum_{s=1}^{n} \nu_{k,s}'' g_s^* - \sum_{s=1}^{n} \nu_{k,s}' g_s^* \tag{22}$$

The species Gibbs free energy g_s are obtained from tables in Ref. [15]. In the present study the reactions 5,6 and 7 have been "turned off" so as to treat N_2 as an inert gas.

Turbulence Modelling

The algebraic turbulence model proposed by Baldwin and Lomax [20] is used in the present code for turbulent calculations. This model was chosen for its inherent simplicity and its suitability for complex flows with length scales that are not well defined. For three-dimensional internal corner flows, the turbulence model is modified as proposed by Hung *et al.* [21]. Using the computed eddy viscosities, the thermal conductivity and mass diffusivity are calculated to account for turbulent mixing. A turbulent Prandtl number of 0.9 is used for all the calculations in the present research.

NUMERICAL METHOD

Gasdynamic Solution

A finite–volume, upwind, TVD scheme is is used to integrate the fluid dynamic equations. The algorithm is second–order accurate in the crossflow plane and first–order accurate in the streamwise marching direction. The upwind algorithm is based on Roe's steady approximate Riemann solver [22] which has been modified [7] for "real gas" effects. The heat flux terms include the effects of mass diffusion. Second–order central differences are used to model the mass diffusion terms. Further details of the algorithm can be found in Refs. [5,9].

Chemistry Solution

The species continuity equation is solved in a loosely–coupled manner using a finite–volume formulation. The requirement that the mass fraction of the species sum to unity eliminates the nth species continuity equation:

$$c_n = 1 - \sum_{s=1}^{n-1} c_s \tag{23}$$

This results in requiring only $n-1$ equations to be solved. The convective terms are modeled using first–order upwind differences and the strong conservation–law form is retained by using the fluid fluxes (the coefficients of the convective terms) as known quantities from the most recent fluid integration step. The species production/depletion rate $\dot{\omega}_s$, is treated as a source term and is lagged to the nth marching station for the present calculations.

A line Gauss–Seidel procedure with successive over–relaxation (SOR) is used to solve each equation. A scalar tridiagonal solver is used to solve the resulting system of equations in an iterative manner until the residual drops below a specified tolerance level ε. The residual is defined as

$$| c_s^{i+1} - c_s^i | \leq \varepsilon$$

where $i+1$ is the current iteration level and i is the previous iteration level.

Fluid/Chemistry Coupling

The coupling between the fluids and chemistry is achieved in an approximate manner. The fluid step is first taken with frozen chemistry to advance from the n to the $n+1$ marching station. The fluid density and velocity computed at the new station are then used to advance the chemistry solution to the $n+1$ level. After determining the species mass fractions, mixture molecular weight, fluid density and internal energy at the $n+1$ level, the new pressure, temperature, γ, specific enthalpy and frozen specific heats are calculated.

The temperature is obtained using the following Newton–Raphson iterative scheme

$$T^{*^{k+1}} = T^{*^k} - \frac{\mathcal{F}(T^{*^k}) - e^*}{\mathcal{F}'(T^{*^k})} \tag{24}$$

where

$$\mathcal{F}(T^{*^k}) = \sum_{s=1}^{n} c_s \left(h_s^*(T^*) - \frac{\mathcal{R}_U T^*}{\mathcal{M}_s^*} \right) \tag{25}$$

$$\mathcal{F}'(T^{*^k}) = \sum_{s=1}^{n} c_s \left(C_{p,s}^*(T^*) - \frac{\mathcal{R}_U}{\mathcal{M}_s^*} \right) \tag{26}$$

and k is the iteration level. The iterations are continued until

$$| T^{k+1} - T^k | \leq \delta$$

where δ is a specified tolerance level. Once the temperature is determined, the pressure can be found from Eq. 10 and γ from Eq. 11.

The coupling between the fluids and chemistry can be enhanced through the implementation of Newton iterations on the governing equations at each streamwise step [9]. However, this was found not to be necessary for the cases considered in this study.

NUMERICAL RESULTS

The new internal flow UPS code has been used to compute two test cases. The two test cases were chosen to demonstrate and validate the hydrogen–air combustion as well as the

three–dimensional internal flow capability of the code. The first test case is the Burrows–Kurkov supersonic combustion experiment [13] and the second one is a three-dimensional, internal flow, shock induced combustion case which simulates a generic 3–D scramjet flow-field.

Test Case 1:

In the two-dimensional Burrows–Kurkov experiment [13], combustion occurs in the supersonic shear layer produced by the sonic injection of hydrogen into a stream of vitiated air. The test section consists of two nearly parallel walls with the lower wall slightly angled down. A schematic of the experimental setup is shown in Fig. 1. The freestream conditions for the hydrogen jet and the vitiated air are given in Table 2 and the wall temperature was held constant at 298°K.

Freestream	H_2 jet	Vitiated airstream
Mach number	1.0	2.44
Temperature, °K	254.0	1270
Pressure, atm	1.0	1.0
H_2 mass fraction	1.0	0.0
H_2O mass fraction	0.0	0.256
O_2 mass fraction	0.0	0.258
N_2 mass fraction	0.0	0.486

Table 2: Freestream conditions for Burrows–Kurkov experiment

For all the calculations, a grid consisting of 101 grid points in the normal direction was used. The grid was clustered near the lower wall in order to properly resolve the shear layer. The first point off the wall was placed at 1.0×10^{-8}m. The Baldwin–Lomax turbulence model was employed to simulate turbulent mixing.

Two computations were performed with the first one being a pure mixing case. For both computations, freestream startup conditions were assumed at the x=0 plane. In the

mixing case only, the freestream temperature was set to 1150°K to match the experiment [13] and all of the O_2 in the vitiated air region was replaced by N_2 so that no combustion takes place. The species mole fraction profiles at the exit plane (x=35.6 cm) are compared with the experimental results in Fig. 2. The computed results are in excellent agreement with the experimental results. The second calculation used the flow conditions listed above which allow supersonic combustion to occur. Ignition, based on the mass fraction of OH species, was found to occur at about 15cm. The species mole fraction profiles at the exit plane are compared with the experimental results in Fig. 3. The flame strength denoted by the peak in the H_2O profile and the wall mole fraction values agree well with the experimental predictions but the species profiles are shifted closer to the lower wall. A series of grid refinement studies were performed and no appreciable change in the behavior of the profiles was found. This issue is currently being investigated further. The total temperature profiles at the exit station are compared in Fig. 4. The computed results, including the peak total temperature location and magnitude, compare well with the experimental data.

Test Case 2:

The second test case consists of a three–dimensional duct with a 15 degree compression ramp. Air, pre–mixed with hydrogen, enters the duct with a freestream Mach number of 7. Combustion occurs as a result of the shock emanating from the compression ramp. The schematic of the 3–D duct is shown in Fig. 5. The side walls have been removed for the sake of clarity. The freestream flow conditions are given in Table 3. The flow is assumed to be turbulent and a constant wall temperature of 500°K is used. A grid consisting of 61×61 points at each marching station was clustered at all four walls to properly resolve the turbulent boundary layer. Due to the presence of the strong shock, smaller streamwise step sizes were taken in the vicinity of the compression corner.

The contours in the centerline, streamwise plane for Mach number and H_2O mole fraction are shown in Figs. 6 and 7, respectively. As expected the strong compression shock

Mach number	7.0
Reynolds number, /m	1.013×10^6
Temperature, °K	1200.0
H_2 mass fraction	0.03207
O_2 mass fraction	0.25447
N_2 mass fraction	0.71346

Table 3: Freestream conditions for 3–D case

emanating from the corner induces combustion. The profiles of pressure, temperature and H_2O mole fraction at the centerline of the exit plane (x=3cm) are shown in Figs. 8, 9 and 10, respectively. Once again it is clearly seen that the compression due to the shock increases the pressure and temperature and initiates the reactions to produce water vapor.

CONCLUDING REMARKS

The three–dimensional UPS code has been extended in the present grant to solve internal turbulent flows with hydrogen–air chemistry. The code now has the capability to compute external or internal flows with either perfect gas, equilibrium air, nonequilibrium air, or nonequilibrium hydrogen–air chemistry. As a consequence, this code can now be used to compute the integrated aerodynamic/propulsive flowfields of hypersonic vehicles such as the NASP.

REFERENCES

[1] Prabhu, D. K., Tannehill, J. C. and Marvin, J. G.,"A New PNS Code for Chemical Nonequilibriun Flows," AIAA Paper 87–0248, January 1987; also *AIAA Journal*, Vol. 26, No. 7, July 1988, pp. 808–815.

[2] Prabhu, D. K., Tannehill, J. C. and Marvin, J. G.,"A PNS Code for Three–Dimensional Chemically Reacting Flows," AIAA Paper 87–1472, June 1987; also *Journal of Thermophysics and Heat Transfer*, Vol. 4, No. 3, July 1990, pp. 257–258.

[3] Wadawadigi, G.,"Computation of Three–Dimensional Chemically Reacting Flows Using a Fully–Coupled, Shock–Fitting PNS Code," M.S. Thesis, Iowa State University, 1989.

[4] Lawrence, S. L., Tannehill, J. C. and Chaussee, D. S.,"An Upwind Algorithm for the Parabolized Navier–Stokes Equations," AIAA Paper 86–1117, May 1986; also *AIAA Journal*, Vol. 27, No. 9, Sept. 1989, pp. 1175–1183.

[5] Lawrence, S. L., Chaussee, D. S. and Tannehill, J. C.,"Application of an Upwind Algorithm to the Three–Dimensional Parabolized Navier–Stokes Equations," AIAA Paper 87–1112, June 1987; also *AIAA Journal*, Vol. 28, No. 6, June 1990, pp. 971–972.

[6] Tannehill, J. C., Ievalts, J. O. and Lawrence, S. L.,"An Upwind Parabolized Navier–Stokes Code for Real Gas Flows," AIAA Paper 88–0713, January 1988.

[7] Tannehill, J. C., Ievalts, J. O., Prabhu, D. K. and Lawrence, S. L., "An Upwind Parabolized Navier–Stokes Code for Chemically Reacting Flows," AIAA Paper 88–2614, June 1988; also *Journal of Thermophysics and Heat Transfer*, Vol. 4, No. 2, April 1990, pp. 149–156.

[8] Tannehill, J. C., Buelow, P. E., Ievalts, J. O. and Lawrence, S. L., "A Three–Dimensional Upwind Parabolized Navier–Stokes Code for Real Gas Flows," AIAA Paper 89–1651,

June 1989; also *Journal of Spacecraft and Rockets*, Vol. 27, No. 2, March–April 1990, pp. 150–159.

[9] Buelow, P. E., Tannehill, J. C., Ievalts, J. O. and Lawrence, S. L., "A Three–Dimensional Upwind Parabolized Navier–Stokes Code for Chemically Reacting Flows," AIAA Paper 90–0394, January 1990; also *Journal of Thermophysics and Heat Transfer*, Vol. 5, No. 3, July–Sept. 1991, pp. 274–283.

[10] Grossman, B. and Walters, R. W.,"An Analysis of Flux–Split Algorithms for Euler's Equations with Real Gases," AIAA Paper 87–1117–CP, June 1987.

[11] Ievalts, J. O., Buelow, P. E. and Tannehill, J. C.,"Comparison of Three–Dimensional Nonequilibrium PNS Codes," AIAA Paper 90–1572, June 1990.

[12] NASP Rate Constant Committee, "Hypersonic Combustion Kinetics: Status Report Of The Rate Constant Committee," NASP High Speed Propulsion Technology Team, NASP TM–1107, 1990.

[13] Burrows, M. C. and Kurkov, A. P. "Analytical and Experimental Study of Supersonic Combustion of Hydrogen in a Vitiated Airstream." NASA TM X–2828. 1973.

[14] Vigneron, Y. C., Rakich, J. V. and Tannehill, J. C., "Calculation of Supersonic Flow over Delta Wings with Sharp Subsonic Leading Edges." AIAA–78–1137. Fluid Dynamics and Plasma Dynamics Conference, July 10-12, 1978, Seattle, Washington.

[15] McBride, B. J., Heimel, S., Ehlers, J. G., and Gordon, S., "Thermodynamic Properties to 6000°K for 210 Substances Involving the First 18 Elements." NASA SP–3001. 1963.

[16] Svehla, R. A., "Estimated Viscosities And Thermal Conductivities Of Gases At High Temperatures." NASA TR R–132. 1962.

[17] Wilke, C. R., "A Viscosity Equation for Gas Mixtures." *Journal of Chemical Physics*, 18(April 1950): 517.

[18] Strehlow, R. A., "*Combustion Fundamentals.*" New York: McGraw-Hill Book Company, 1984.

[19] Gardiner, W. C. Jr., "*Combustion Chemistry.*" New York: Springer–Verlag, 1984.

[20] Baldwin, B. S. and Lomax, H. "Thin Layer Approximation and Algebraic Model for Separated Turbulent Flows." AIAA–78–257. Aerospace Sciences Meeting, Jan. 16–18, 1978, Huntsville, Alabama.

[21] Hung, C. –M. and Buning, P. G. "Simulation of Blunt–Fin–Induced Shock–Wave and Turbulent Boundary–Layer Interaction." *Journal of Fluid Mechanics*, 154(1985): 163–185.

[22] Roe, P. L. "Approximate Riemann Solvers, Parameter Vectors, and Difference Schemes," *Journal of Computational Physics*, 43(1983): 357–372.

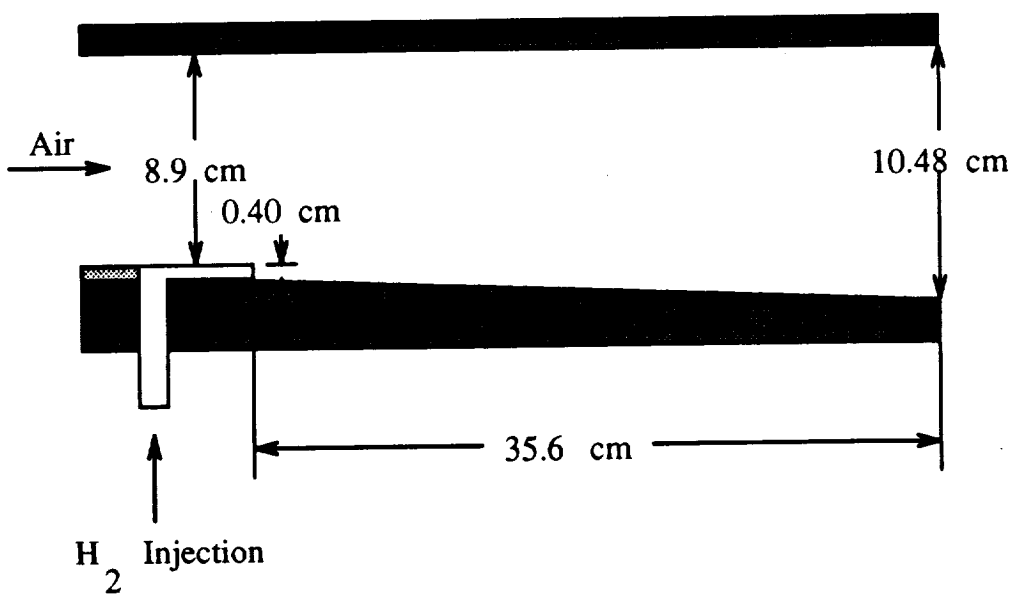

Figure 1: Schematic of the Burrows–Kurkov experimental setup

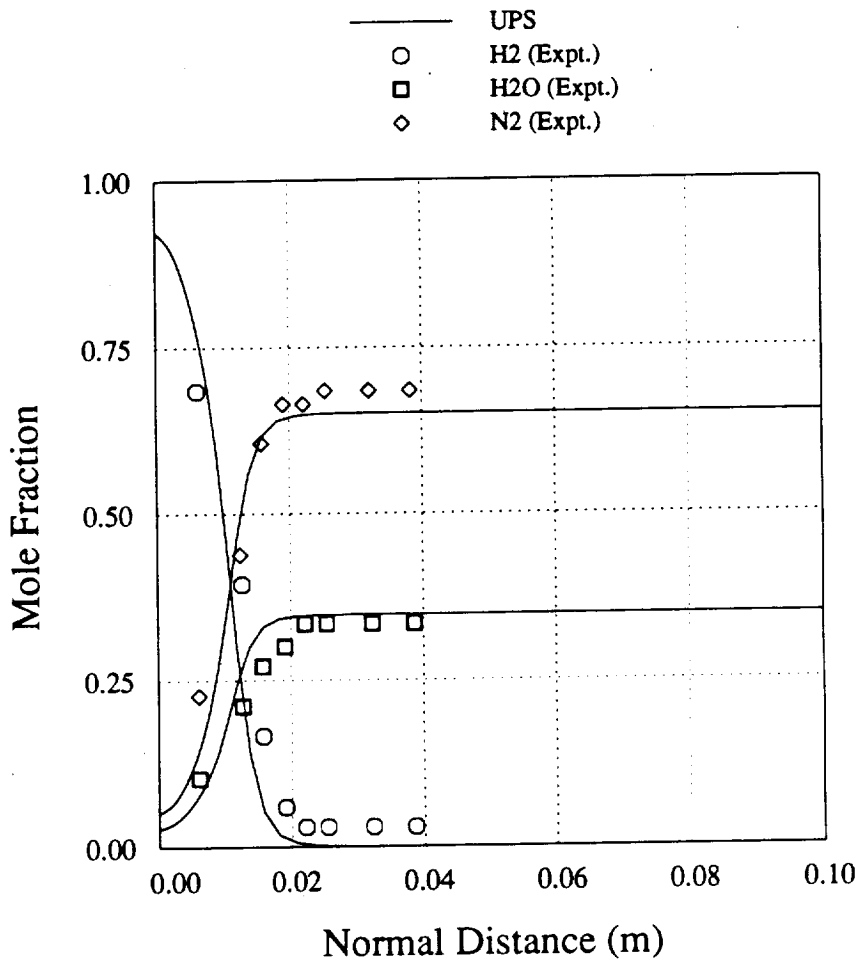

Figure 2: Species mole fraction profiles at the exit plane (x=35.6cm; pure mixing case)

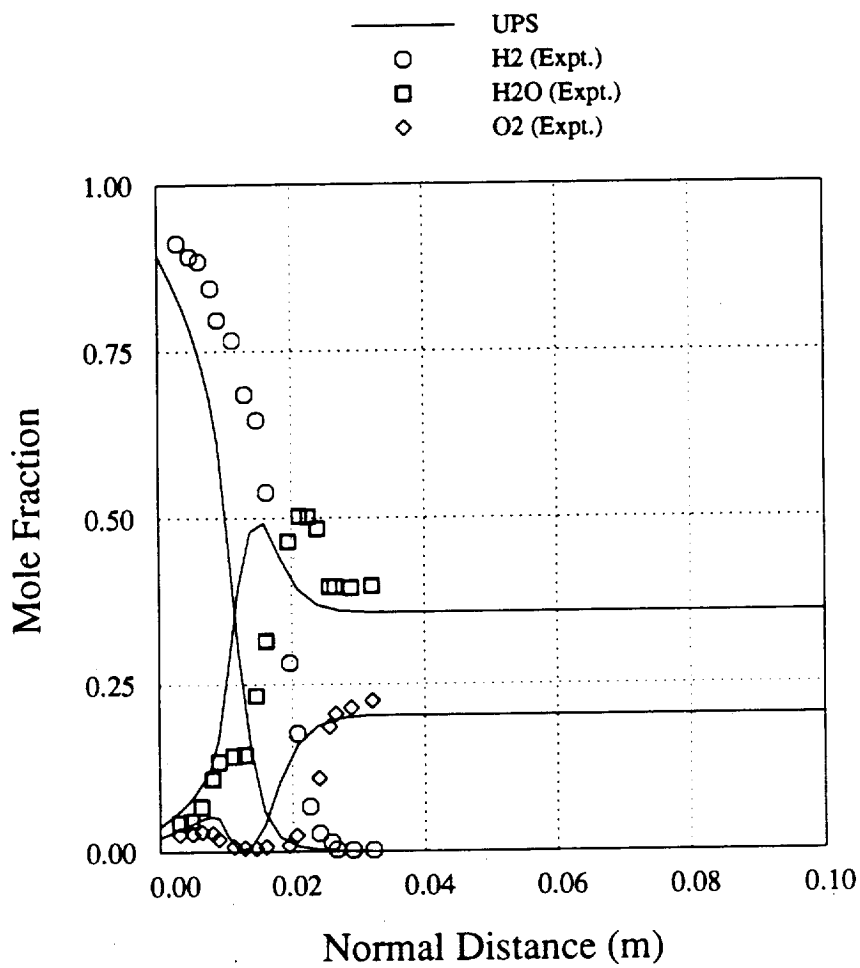

Figure 3: Species mole fraction profiles at the exit plane (x=35.6cm; combustion case)

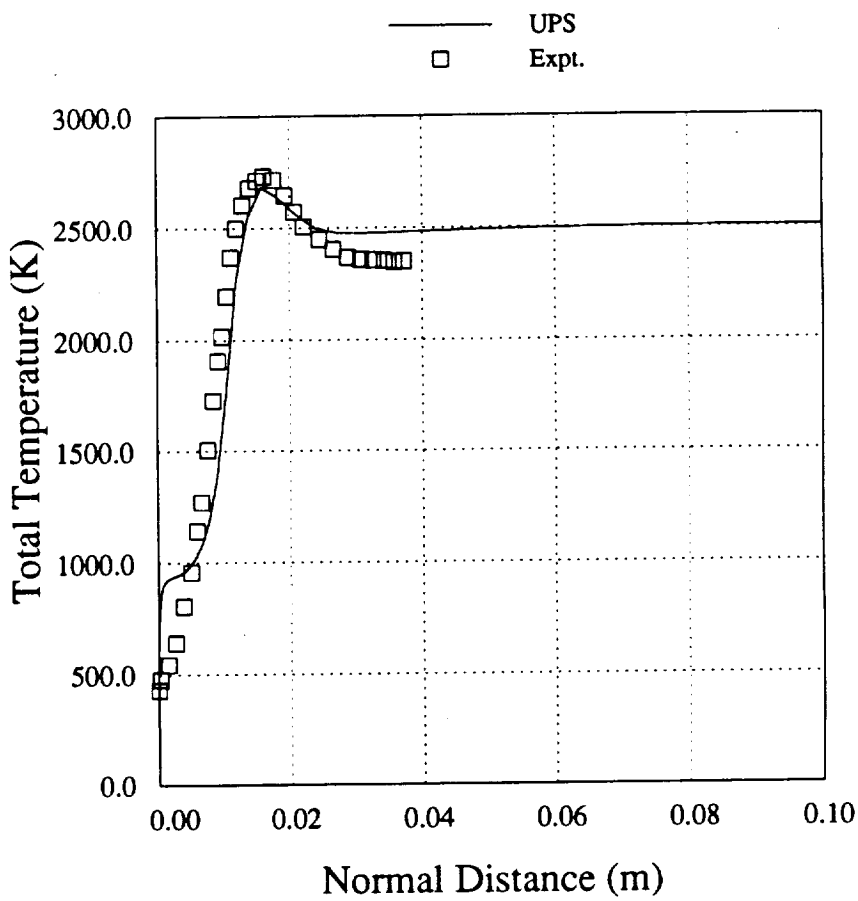

Figure 4: Total temperature profiles at the exit plane (x=35.6cm; combustion case)

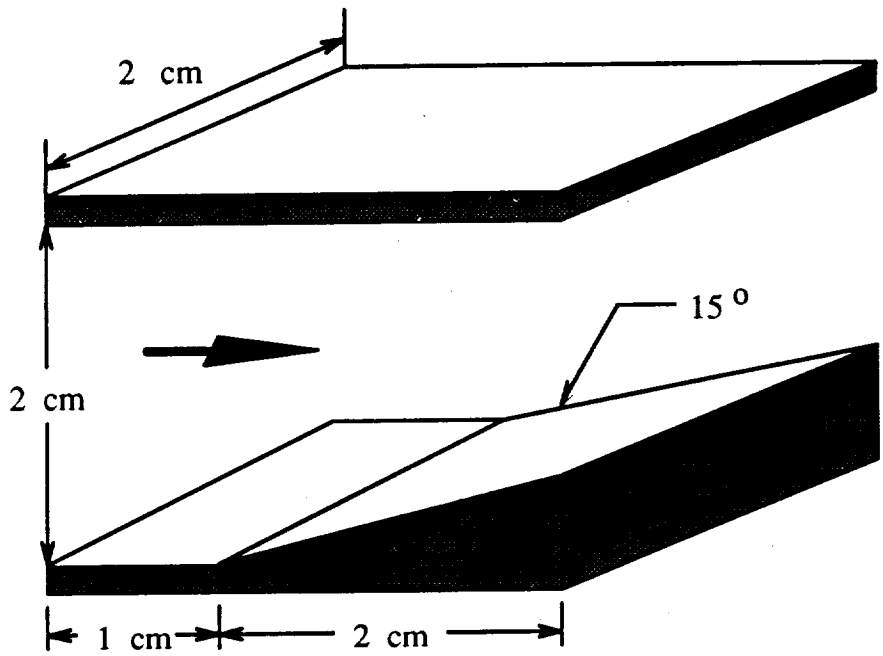

Figure 5: Schematic of the 3–D duct

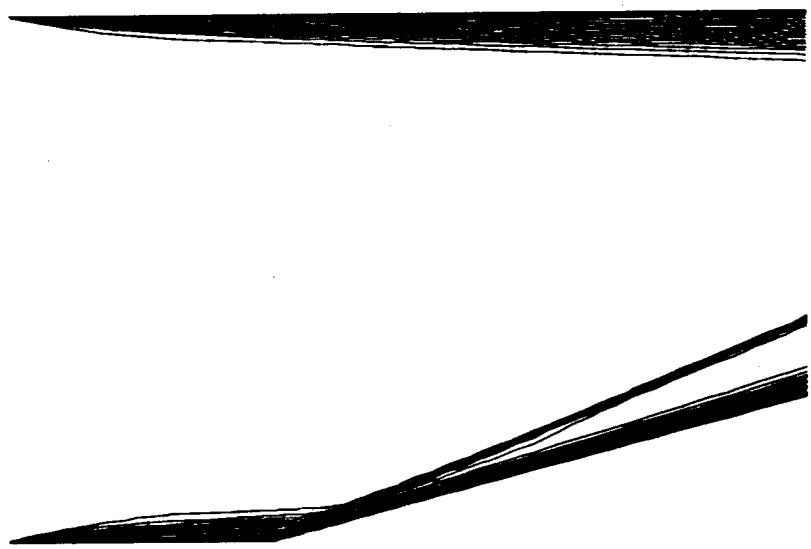

Figure 6: Mach contours in the centerline streamwise plane